Occurrence and characteristics of rock glaciers in the Poiqu River basin – Central Himalaya

Philipp Rastner[a,b]*, Tobias Bolch[c*], Yan Hu[d], Lin Liu[d], Atanu Bhattacharya[c,e], Guoqing Zhang[f] and Tandong Yao[f]

[a]Department of Geography, University of Zurich, Switzerland; [b]GeoVille Information Systems and Data Processing GmbH, Innsbruck, Austria, [c]School of Geography and Sustainable Development, University of St. Andrews, Scotland, UK; [d]Earth System Science Programme, The Chinese University of Hong Kong, Hong Kong, China; [e]Department of Remote Sensing and GIS, JIS University, Kolkata, India; [f]Institute of Tibetan Plateau Research, Chinese Academy of Sciences, China

*corresponding author: philipp.rastner@geo.uzh.ch, tobias.bolch@st-andrews.ac.uk

Occurrence and characteristics of rock glaciers in the Poiqu River basin – Central Himalaya

Rock glaciers are important to study as they can be of hydrological importance and could have serious hazard potentials. Existing investigations about rock glaciers in High Mountain Asia indicate that the landforms are abundant, but information is still rare for large parts of the region. We compiled a rock glacier inventory for the Poiqu River basin, Central Himalaya. The mapping was conducted using very high-resolution Pléiades imagery and digital elevation model and imagery available from Google Earth. Rock glaciers were classified either active or inactive based on interferograms generated using ALOS-1 PALSAR data. Moreover, we developed a new method to automatically map the frontal slopes of the rock glaciers to investigate their activity. The results reveal 370 rock glaciers including 148 active and 222 inactive ones. We found nine rock glaciers damming lakes, three of which could be potentially dangerous. The overall rock glacier area is about 20.9 km^2 which is more than 10% of the glacier area. The two largest rock glaciers cover 0.50 and 0.45 km^2. The rock glaciers are located at elevations between ~4000 and ~6000 m above sea level (mean elevations ~5100 m). Most of the rock glaciers face towards East and Southwest. The mean overall slope is 19.3° with the active ones being on average only slightly steeper (active: 19.7°, inactive: 19.0°). Their frontal slopes, however, are clearly steeper. The availability of very high-resolution data was key to generate a rock glacier inventory and allowed assessment of the rock glacier characteristics with high accuracy.

Keywords: Himalaya; Tibet; Pléiades; InSAR; Digital Elevation Model (DEM), rock glacier inventory; frontal slopes

Introduction

Rock glaciers are distinctive geomorphological landforms, consisting of angular rock and ice which creep slowly downward due to gravity (Barsch 1996; Humlum 2000; Haeberli *et al.* 2006). Different opinions regarding the origin of the ice have been proposed but it is commonly accepted that rock glaciers are related to permafrost occurrence. A widely accepted definition is that active rock glaciers are “the visible

expression of cumulative deformation by long-term creep of ice/debris mixtures under permafrost conditions" (Berthling 2011). Rock glaciers typically display a complex transversal ridge-and-furrow structure due to compressive flow and are sometimes associated elongated ridges parallel to the flow (Haeberli *et al.* 2006). Rock glaciers are important geomorphological transport systems and can have a relevant contribution to water supply and alter river runoff (Jones, Harrison, Anderson and Betts 2018; Brighenti *et al.* 2019). Moreover, rock glaciers have been documented to cause mass waste hazards on steep mountain slopes, threatening sensible infrastructure in some downhill areas (Kääb *et al.* 2005; Schoeneich *et al.* 2015).

Rock glaciers are commonly classified into three groups according to their kinematic status and amount of the internal ice: active, inactive and relict ones (Barsch 1996). Active rock glaciers are moving down-slope or down-valley (in the order of decimetres to a few meters per year). When the movement decreases because of ice loss in the body or due to decreasing rock and debris supply, rock glaciers become inactive. Relict rock glaciers still present the shape of a rock glacier but display much smaller volumes due to the loss of ice in its body. In addition, clear collapse structures are visible and typically vegetation already covers the surface (Barsch 1996; Berger *et al.* 2004; Bishop *et al.* 2004; Haeberli *et al.* 2006; Necsoiu *et al.* 2016).

The activity of rock glaciers can be measured by in-situ observations or by remote sensing including feature tracking of optical images (e.g. (Kääb *et al.* 1997; Kääb *et al.* 2021), Interferometric Synthetic Aperture Radar (InSAR) measurements or a coherence index from active sensors (Barboux *et al.* 2014; Bollmann *et al.* 2015; Bertone *et al.* 2019)

In many studies, however, the activity has been presumed from the following surface features (Wahrhaftig and Cox 1959; Blagbrough and Farkas 1968; Imhof 1996;

Burger *et al.* 1999; Falaschi *et al.* 2014): Active rock glaciers have a steep (>35°) vegetation-free frontal slope and load fresh-looking and unstable boulders on the upper surface. In contrast, inactive rock glaciers show a gentler frontal slope with partial or full vegetation. The latter also presents a well-developed boulder apron at the foot of the frontal slope and stable boulders on the upper surface. In contrast, inactive rock glaciers show on average a gentler frontal slope with initial vegetation.

Depending on the location, rock glaciers can additionally be separated into a) moraine-derived rock glaciers and b) talus-derived rock glaciers. The former develops beneath the terminal moraines of glaciers and transports mainly reworked glaciogenic materials (Lilleøren *et al.* 2013; Scotti *et al.* 2013). The latter develop below talus slopes and have no visible ice upslope. These landforms transport mainly rock fragments generated from the adjacent rock walls (Lilleøren *et al.* 2013; Scotti *et al.* 2013). The latter develop below talus slopes have no visible ice upslope. These landforms transport mainly rock fragments generated from the adjacent rock walls (Lilleøren and Etzelmüller 2011).

The knowledge about rock glaciers improved in recent years in particular for the European Alps (Cremonese *et al.* 2011; Kellerer-Pirklbauer *et al.* 2012; Krainer and Ribis 2012; Scotti *et al.* 2013), Andes (Esper Angillieri 2009; Falaschi *et al.* 2014; Rangecroft *et al.* 2014; Falaschi *et al.* 2015), Carpathian mountains (Onaca *et al.* 2017) as well as in High Mountain Asia including the Tibetan mountains and the Himalaya (Schmid *et al.* 2015; Jones, Harrison, Anderson, Selley *et al.* 2018; Reinosch *et al.* 2021) and the Tien Shan ((Bolch and Gorbunov 2014; Wang *et al.* 2017; Blöthe *et al.* 2019; Bolch *et al.* 2019). The only region where detailed knowledge about rock glacier characteristics and occurrence existed already several decades ago is the Northern Tien Shan (Titkov 1988; Gorbunov and Titkov 1989; Gorbunov *et al.* 1992; Gorbunov *et al.*

1998). Nevertheless, for large areas in HMA, e.g. for the most parts of the Himalaya located in Tibet, information about rock glaciers is sparse or not available, even though existing information shows that rock glaciers are abundant (Jones, Harrison, Anderson and Betts 2018; Reinosch *et al.* 2021). Moreover, mapping approaches and definitions are also varying amongst these studies.

The main aims of this work are (i) to apply a consistent and integrative method to map and classify rock glaciers for the whole Poiqu River basin in central Himalaya in Tibet by using high resolution optical images together with InSAR measurements and a high-resolution digital elevation model, (ii) to test whether information about rock glacier activity can also be automatically derived from the frontal slope, and (iii) to analyse the characteristics of rock glacier occurrence and put them into the wider context of existing studies.

Study Region

The Poiqu River basin is located in central Himalaya, drains from the Tibetan Plateau into the Bote Koshi/sun Koshi watershed in Nepal and has an area of ~2000 km^2 (Fig. 1). The mean elevation of the study region is about 4900 m above sea level (asl.), with the maximum elevation being Shishapangma (8024 m asl.) and the lowest elevation measured at Friendship Bridge at the border to Nepal (1540 m asl.). Consequently, the mean annual air temperature is relatively low (3.8°C between 1967 and 2017 at Nyalam weather station, 3750 m asl. (Zhang *et al.* 2019). The temperature showed a warming trend of 0.024 °C/yr , and precipitation a decreasing trend of -0.76 mm/yr during 1967−2017 from station observations (Zhang *et al.* 2019). Glaciers in this basin cover approximately 190 km^2 (in 2015) (Zhang *et al.* 2019) and preliminary assessments during field work confirmed the presence of rock glaciers (Fig. 2). The Nyalam region has strong tectonic deformation and is a classic area for studying the

Himalaya orogenic belt. The tectonic unit is the high Himalayan crystalline basement mafic belt. The strata are pre-Sinian medium-deep metamorphic Nyalam Group and Nuqiecun Group (Li *et al.* 2006). Since the opening of the Kodari Highway along the valley, which links Kathmandu (Nepal) with Lhasa in Tibet/China, international trade and tourism between the two countries have been growing rapidly. About 200,000 people live in the area whose major source of income is agriculture (Khanal *et al.* 2015).

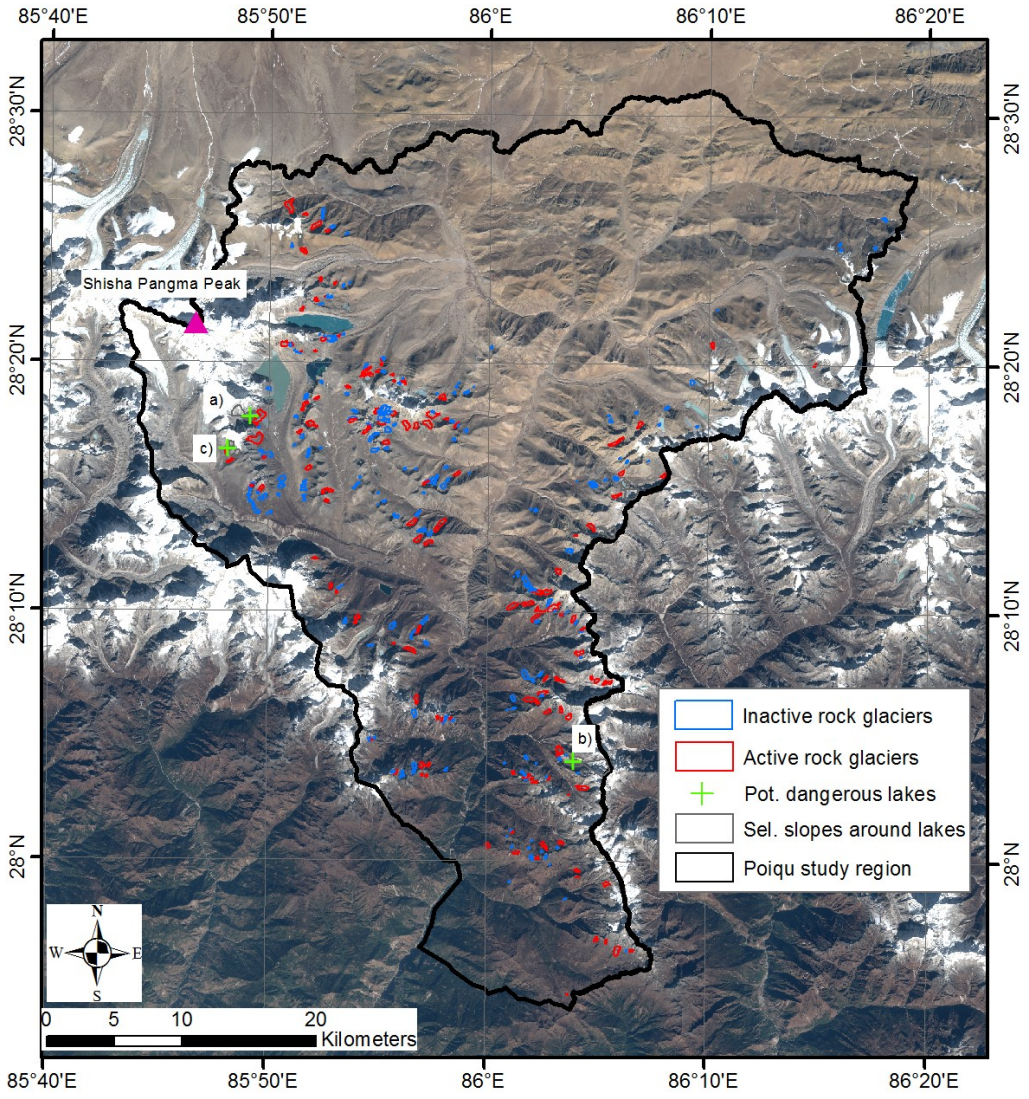

Fig. 1: Rock glacier inventory for the Poiqu River basin (central Himalaya) and identified potentially dangerous lakes dammed by a rock glacier. Background image: Sentinel-2, acquired 12.09.2016.

Fig 2: Two rock glaciers in the Poiqu basin. Left: moraine-derived rock glacier also displayed in Fig. 3 (Photo: J. B. Pronk, 2019). Right: Talus-derived rock glacier (Photo: T. Bolch, 2018).

Data and data pre-processing

Pléiades optical satellite imagery

We acquired very high resolution Pléiades imagery, an optical earth observation system developed by the French Space Agency (CNES). Pléiades 1A and 1B, launched on 17th December 2011 and 2nd December 2012 respectively, consist of similar but not identical satellites that are placed at an altitude of 694 km. Pléiades comprises twin satellites that can produce multispectral and panchromatic images. The nadir resolution of the panchromatic and multispectral bands are 0.7m and 2.8m and resampled to 0.5m and 2.0m respectively (Gleyzes *et al.* 2012). Moreover, the panchromatic band has a radiometric resolution of 12 bits, considerably higher than ASTER and SPOT-5 (each 8 bits), which provides better contrast in order to perform image matching in low contrast surfaces such as fresh snow or cast shadows. Pléiades offers an image swath of 20 km at nadir, and by adapting its viewing angle of up to 47°. The oblique viewing capability allows the satellites to revisit any point on the globe daily. Pléiades can also provide tri-stereo facility, acquisition of three images focusing on the same area at one single pass

under different incidence angles, which makes us possible to generate multiple DEMs for the same scene for comparison (Durand *et al.* 2013).

Ten different Pléiades 1A and1B tri-stereo images had to be acquired to cover the whole basin. The images were taken between 25th September 2018 and 4th November 2018 (Table 1). The images are provided in Dimap format and processed at level 1A with a base-to-height (b/h) ratio for their stereoscopic pairs ranging from 0.20 to 0.48. We have orthorectified all the Pléiades nadir viewing images (0.5m spatial resolution) and then image mosaiced all of them based on their DEMs (1m spatial resolution) derived from the same stereo imagery.

Digital Elevation Models

To retrieve topographic parameters as well as supporting rock glacier mapping, we generated DEMs from the Pléiades tri-stereo bundle images. Along with Pléiades images, Rational Polynomial Coefficients (RPC) are distributed which provide the relationship between ground points and corresponding image points. DEMs were extracted with the software package Orthoengine of PCI Geomatica 2018 using RPC function model. We identified an average of ten well-distributed ground control points (GCPs) for each tri-stereo pair to perform the planimetric adjustment with a RMSE errors within < 1 pixels in x and y directions. GCPs were collected from Sentinel-2 multispectral images (10 m spatial resolution) with the SRTM DEM (version 3.0 global 1 arc second, 30m spatial resolution) as vertical reference. In order to improve the sensor model, one hundred tie points were generated using normalized cross correlation image matching algorithm for all combination of images, such as, backward, nadir and forward. Tie points with residuals less than one pixel resolution (average RMSE of 0.25 pixels and 0.39 pixels in x and y directions respectively) were used for bundle block adjustment. After bundle block with first order RPC adjustment, the residuals of the

GCPs in the stereo model were on average 0.30 m 0.24 m in x and y directions respectively. We calculated three epi-polar pairs from forward, nadir and backword looking views. Then, we used the Semi Global Matching (SGM) algorithm with a high smoothing filter to generate DEMs of 1 m spatial resolution. Finally, all DEMs were mosaicked.

We used the NASA Shuttle Radar Topography Mission (SRTM) Version 3.0 Global 1 arc second DEM product for correcting topographic phases and geocoding in the InSAR analysis. The SRTM DEM was acquired during Feb 2000, with a spatial resolution of approximately 30 m. The nominal absolute height accuracy of the product is < 16 m (Farr *et al.* 2007).

Table 1: An overview of the data used in this study

Dataset	Type	Resolution	Date	Source
Pléiades	Optical	0.5 m	25.09.2018 – 04.11.2018	AIRBUS Geostore
Pléiades DEM	Optical	1m	25.09.2018 – 04.11.2018	Pléiades tri-stereo data
SRTM DEM	Radar	30 m	11.02.2000 – 22.02.2000	https://lpdaac.usgs.gov/products/srtmgl1v003/
ALOS-1 PALSAR	Radar	10 m	16.07.2007 31.08.2007 16.10.2007 16.01.2008 02.03.2008 02.06.2008 18.07.2008	https://ims1d.palsar.ersdac.or.jp/palsar_ims1_public/ims1/pub/en

Radar Satellite Imagery

We computed a total of four differential SAR interferograms from the ALOS-1 PALSAR fine-beam frames, with baselines shorter than 1000 m (Table 2). These

interferograms were processed in the two-pass approach with the InSAR Scientific Computing Environment (ISCE) package (Rosen *et al.* 2012). Standard processing steps included co-registration of the SAR acquisitions, multi-looked interferogram generation (2 looks in range and 5 looks in azimuth), estimation and removal of the topographic phase, filtering with a power-spectral filter and terrain corrected geocoding. Adopting the vertical accuracy of the DEM product as 16 m and the maximum perpendicular baseline as 1000 m, we can estimate that the residual topographic phase would be smaller than 1.8 radians, corresponding to about 3.4 cm in displacement.

Table 2: List of interferograms made from ALOS-1 PALSAR data. Interferogram names are the conjunction of acquisition dates of the two images.

Path/frame	Interferogram	Time span (days)	Perpendicular baseline (m)
509/550	20070716-20070831	46	293
509/550	20080116-20080302	46	487
509/550	20071016-20080602	230	969
509/550	20070716-20080718	368	-832

Methods

Mapping of rock glaciers

Automatic mapping of rock glaciers is challenging, associated with high uncertainties and no standard method exists so far. Although deep learning in combination with object-based image analysis is promising (Robson *et al.* 2020), the manual rock glacier identification and digitisation using high resolution optical data to detect geomorphic indicators remains thus the optimal approach for inventory compilation. Indeed, (Robson *et al.* 2020) used this generated inventory for calibration and validation of their approach. The recently established working group for rock glacier mapping recommends further the use of InSAR data to support rock glacier mapping (IPA Action Group 2020).

In this study we used the high resolution Pléiades images to digitise rock glaciers with distinct front and flanks, manually, as a first step. After that we cross-checked the outlines with the hillshade derived from the 1 m Pleaides DEM. This step helped to refine outlines and sometimes even new rock glaciers could be detected. In addition, we used Google Earth as additional source of information as it allows to see the rock glaciers from different viewing angles and change satellite images from different points in time with various sunlight conditions. InSAR data was considered for the mapping of the rock glaciers, but the signal was most of the time too weak to clearly detect rock glacier outlines. Whereas the determination of the lower limit of the rock glaciers is relatively straightforward, difficulties exist to define and limit the upper boundary (rooting zone). According to (Humlum 1998) and (Sattler *et al.* 2016), it is the zone of the rock glacier where permafrost creep starts, which is usually below 35°. We therefore applied a multiresolution segmentation using an object-based approach (scale: 30, shape: 0.1, compactness: 0.5) within the rock glacier outlines and derived their mean slopes. Finally, we removed all areas, showing slope values of more than 35° in the upper boundaries.

Kinematical and geomorphological classification

In order to classify active and inactive rock glaciers we followed a two-step approach. First, we visually identified the activity of rock glaciers with the help of SAR Interferometry. This technique allows systematic and continuous monitoring of the movement of entire landforms in the satellite line-of-sight (LOS) direction at a scale ranging from individual slope faces to whole mountain ranges (Strozzi *et al.* 2020). Whenever distinct fringes were observable within one rock glacier polygon, we classified them to be active. As a second step, we also checked their activity based on the characteristics of the surface and the frontal slope using the Pléiades data (Fig. 3).

This was necessary as several kinds of errors can be included in SAR interferograms such as decorrelation noise, residual topography contribution and atmospheric delays (Wang *et al.* 2017). Rock glaciers were classified to be active, if distinct flow structures with ridges and furrows at their surface and a fresh-looking front were observable (Strozzi *et al.* 2020).

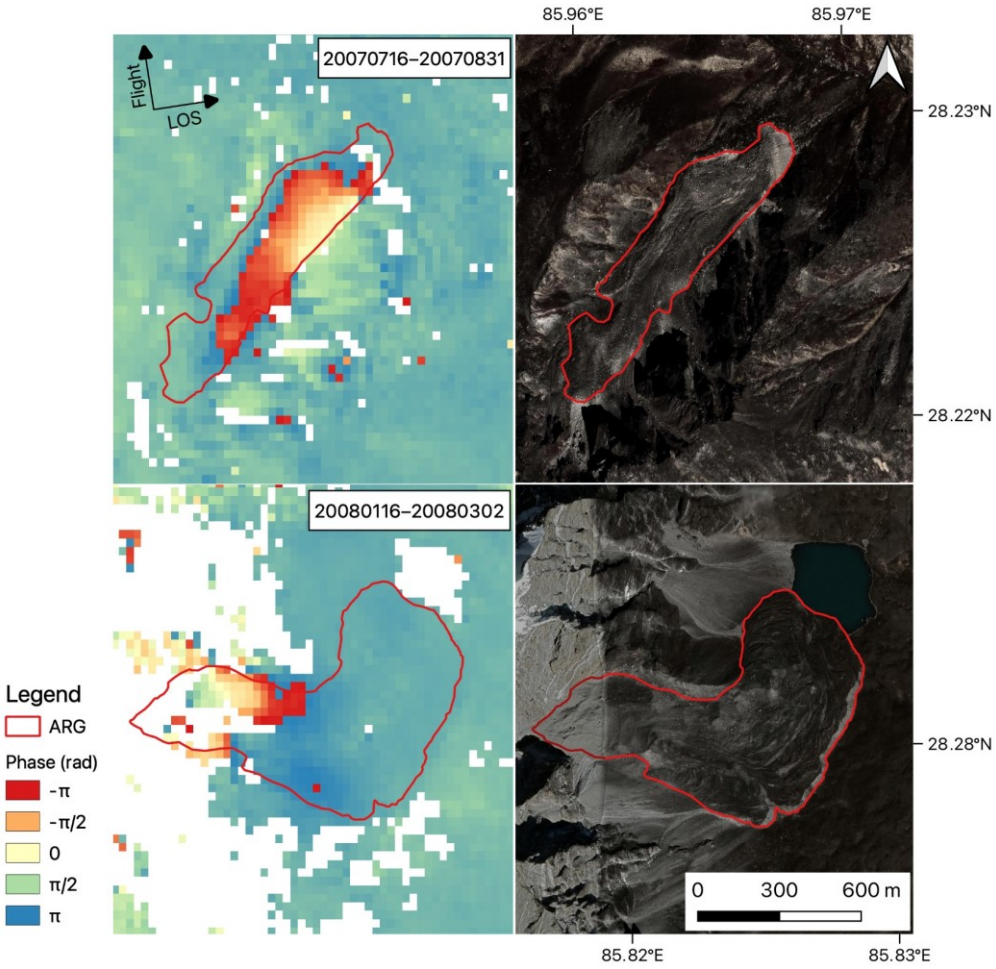

Fig. 3: Kinematic determination with the help of SAR interfereometry for two rock glaciers.

Finally, we also visually classified the rock glaciers in moraine- and talus-derived rock glaciers. Based on their source of rock material, rock glaciers were classified as moraine-derived when they were located beneath the end of moraines of

glaciers and as talus-derived when there was no visible ice upslope and hence likely resulted from transport of rock fragments from adjacent rock walls.

Few rock glaciers are damming or at least partly damming lakes surrounded by steep headwalls. These lakes could release large volumes of water if the rock glacier dam fails and could pose a severe hazard to mountain communities and infrastructure downstream. We therefore also mapped the lateral slopes of the lakes and their headwalls to derive their mean slopes surrounding the lakes.

Rock glacier front slope detection

A further evidence of rock glacier activity is the slope angle of the rock glacier front. As the available data, especially the very high-resolution DEM, allowed to detect and calculate the frontal slope with high accuracy, we a) automatically mapped the front of the rock glaciers in order to extract their slope angles and b) compared the slopes to the visually derived activity to investigate with which accuracy it is possible to detect their kinematic status based on the frontal slopes only. We first set up a processing chain, which performs an object-based multiresolution segmentation to derive the mean slope values over the whole rock glaciers (15°- <20°, 20° - <25°, 25° - <30°, 30° - <35° and > 35°) by using the slope calculated from the 1 m Pleiades DEM and the manually mapped rock glacier inventory. In the next step, the classified slope objects were postprocessed based on context and neighbourhood relationships. In addition, we developed a model in a GIS environment to derive the minimum point of a rock glacier. The model converted the rock glacier area into a raster, appended their corresponding elevation value derived from the Pléaides DEM, and obtained the minimum elevation value for each rock glacier based on summary statistics. Finally, the slope polygons were intersected with the lowest points of each rock glacier (Fig. 4).

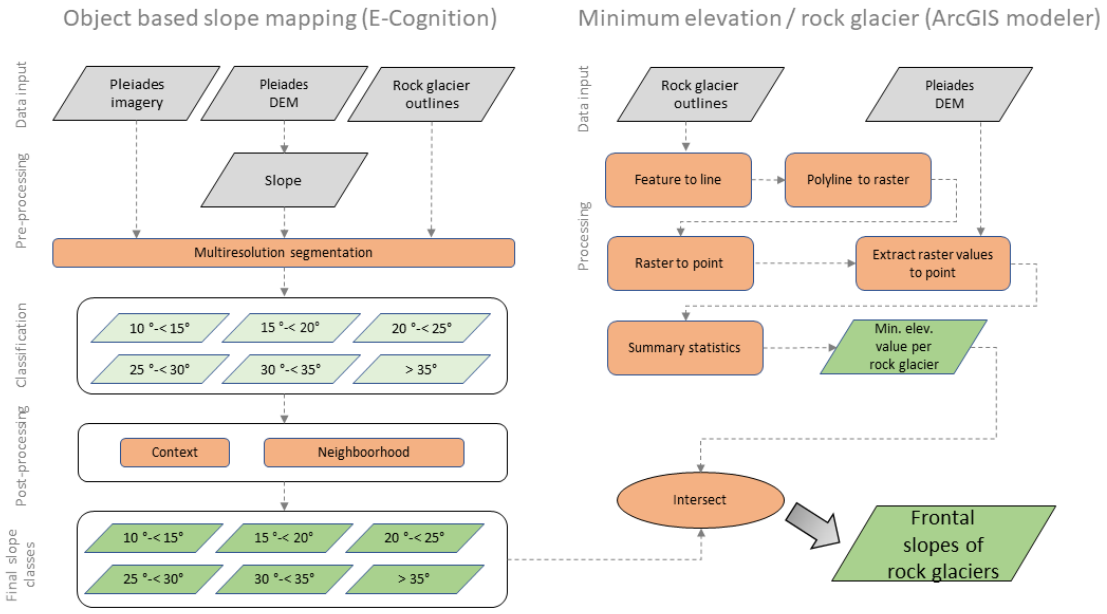

Fig. 4: Schematic overview of the method to derive the frontal slopes of rock glaciers.

Results

Inventory

The results of the inventory reveal 370 rock glaciers covering an area of ~20.9 km2. The two largest rock glaciers have an area of ~0.5 and ~0.45 km² and the next three largest present an area close to 0.3 km^2. The five smallest rock glaciers have an area of less than 0.003 km^2. The mean area of all rock glaciers in the Poiqu River basin is ~ 0.05 km^2. Our study indicates that 148 rock glaciers can be classified as active and represent a total area of 12.5 km^2 (mean area: 0.08 km²) whereas 222 can be classified as inactive with a respective total area of 8.4 km^2 (mean area: 0.04 km²). This means that 40% of the glaciers are active rock glaciers covering ~ 60% of the area of all rock glaciers. Most of the rock glaciers in the study area can be classified as talus-derived rock glaciers (n=297, total area: 15.5 km^2), another part as moraine-derived rock glaciers (n=40, 3.2 km^2) and 33 (2.2 km^2) are not classifiable in neither class. Talus-

derived rock glaciers present overall steeper slopes (19.7°) but are smaller in area (0.05 km^2) than moraine-derived rock glaciers (0.08 km^2, 17.8°).

We found nine sites where rock glaciers are at least partly damming a lake (Fig. 1). From these sites three could be potentially dangerous due to steep slopes and steep glaciers located in the upslope area making rock avalanches which could hit the lake more likely. Lake A is surrounded by a headwall with a mean slope of more than 47°. The Cirenmaco glacial lake (lake B) and lake C have a headwall slope of about 34°. The headwalls of the other lake-damming rock glaciers indicated slopes less than 30° (mean 24°).

The occurrence of rock glaciers shows a correlation with elevation over the whole sample (Fig. 5.). This coincides with decreasing precipitation and increasing average elevation. Around 28° north, the rock glaciers can be found at an elevation of 4000 m, whereas at 28.5° their mean elevation is about 1500 m higher. Focusing on the longitude, we identify a decrease in the mean elevation towards the main valley (west) and an increase again in the east side.

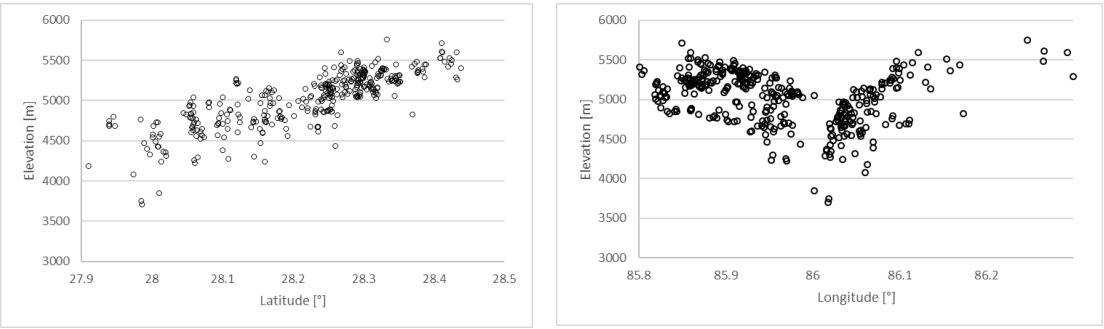

Fig. 5. Relationship between the mean elevation and the latitude (left) and longitude (right) in the study area.

Plotting the area covered and number of glaciers per size class (Fig. 6) reveals a high number of small rock glaciers (size classes from 0-0.06 km^2) which account for

256 rock glaciers in number and only for 6.29 km^2 in area. The two classes of 0.06 to 0.1 km^2 have in both cases the same amount of rock glaciers (~27) but a different area (~1.86; 2.41 km^2). Rock glaciers between 0.1 and 0.2 km2 (n=43) cover an area of more than 5 km^2 and rock glaciers larger than 2 km^2 slightly less than 5 km^2 (n=17).

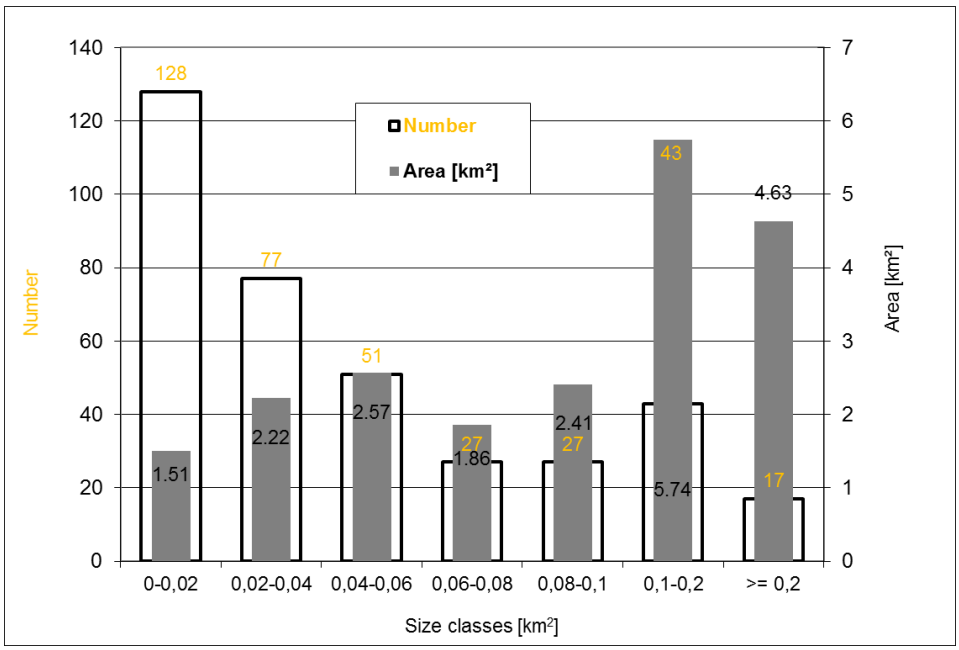

Fig. 6 Number of rock glaciers and area covered per size class

The area-elevation distribution for all, active and inactive rock glaciers shows that they are located between ~4000 m and ~6000 m asl. with a mean elevation of ~5100 m asl. (Fig. 7). The active rock glaciers are located slightly higher (average 5041 m asl.) than the inactive ones (5008 m asl.). The highest active rock glacier was found at an elevation of 5750 m (mean elevation), and its rooting zone at 5797 m whereas the lowest at 3844 m (mean elevation) and its front at 3798 m. The highest inactive rock glacier was found at an elevation of 5708 m (mean elevation) and its rooting zone at 5764 m, whereas the lowest at 3698 m (mean elevation) and its front at 3649 m. In nearly all elevation bins, the area covered by active rock glaciers surpasses that of

inactive rock glaciers. Only in two distinct elevations bins, a) from 4100-4300 m and b) at 4800 m we found more inactive rock glaciers than active ones (Fig. 7).

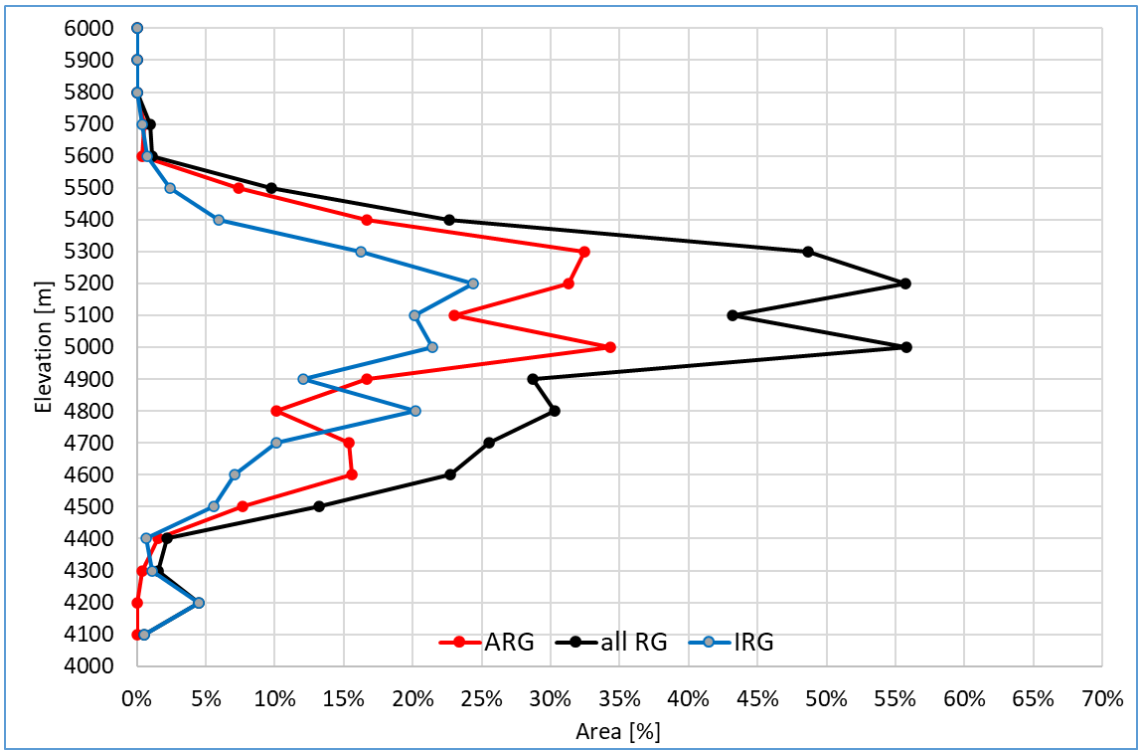

Fig. 7. Area-elevation distribution in 100 m bins for all, active and inactive rock glaciers

More than 17% of all rock glacier area faces towards the E and the SW (> 16%) (Fig. 8). Around 14% of the area faces towards NW and the NE in the respective sectors. The smallest areas can be found in the SE (6.1%) and S (9.1%) sectors. Number wise, the highest amount is detectable in the SW and NE and the lowest amount of rock glaciers are detectable again in SE and E directions. Most of the area and also number of the active rock glaciers can be found in the sectors E and SW. The distribution for the inactive rock glaciers has also a clear peak in the NW (nearly 20%) and a distinct minimum in area in the SE direction (~5%). The largest number of inactive rock glaciers can be found in the NE, W, NW and N (~15%).

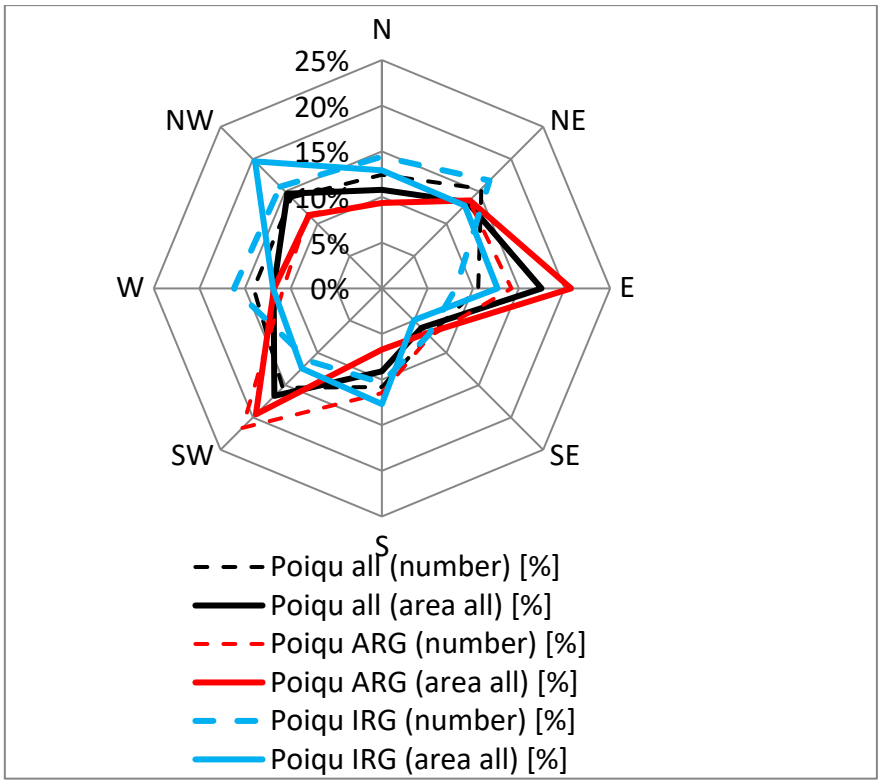

Fig. 8. Area distribution versus aspect per sector for all, active and inactive rock glaciers.

Both active and inactive rock glaciers facing NW have on average about 300 m lower minimum elevations than SE facing ones. One would expect that the active rock glaciers have in all directions higher minimum elevations than inactive ones. This is, however, only true for the NE, E, and SW sectors. In all other sectors, active rock glaciers have always lower or equally high minimum averages.

The mean slope of all rock glaciers is 19.3°, with the active ones being on average slightly steeper (19.7°) than the inactive ones (19.0°). Overall, 321 rock glaciers have a mean slope of less than 25°, forty a slope of between 25° and 30°, seven a slope between 30° and35° and two more than 35°. Only three inactive rock glaciers show a very high mean slope, but they are all small (< 0.01 km2) and are found in steep topography.

The slope angles from the automatically identified fronts range from about 12° to 43° (average ~34°) of the active rock glaciers and from 11° to 38° (average ~24°) og the inactive rock glaciers (Fig. 9). There is a higher number of rock glaciers for the classes 10-20° and a smaller number for 20-30° for both active and inactive rock glaciers. The highest proportion is clearly visible for the classes greater than 30% (Fig. 9). Interestingly, lower slope angles are detectable for all fronts of active rock glaciers inactive rock glaciers in the classes from 10-30°. Above 30°, the frontal slopes of active rock glaciers clearly surpass the inactive ones. The frontal angle thus clearly appears to be steeper on average for active rock glaciers.

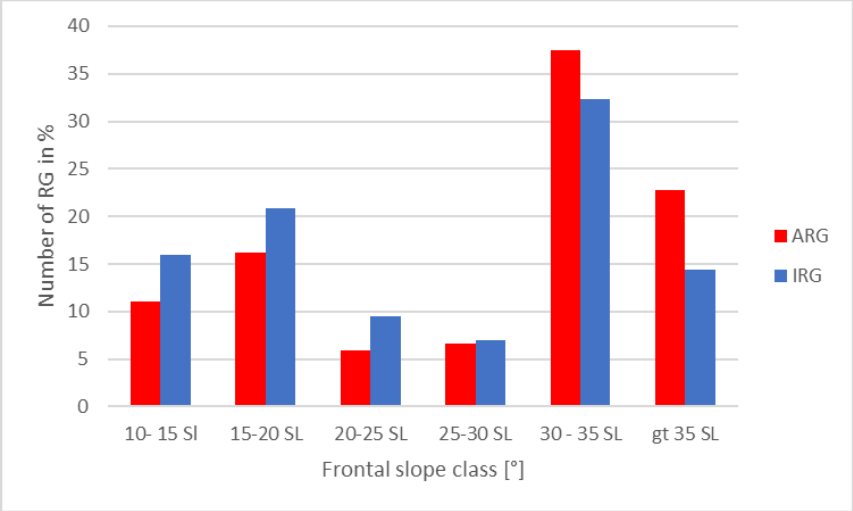

Fig. 9. Mean front slope angles of active and inactive rock glaciers

Discussion

Characteristics of rock glaciers

Our rock glacier inventory of the Poiqu River basin includes 370 rock glaciers which cover an area of 20.9 km^2. Of these 148 (12.5 km^2, 40%) rock glaciers can be classified as active and 222 can be classified as inactive (8.4 km^2, 60%). The rock glacier cover is more than 10% of the glacier coverage and about 1% is of the

investigated region. This is higher than in other parts of the Himalaya (0.6% (Pandey 2019) or north-eastern Tien Shan (0.1% (Wang *et al.* 2017). The rock glacier density is, however, higher in northern Tien Shan in Kazakhstan where the total area of active rock glaciers only represents close to 13% of the glacier coverage (Bolch and Marchenko 2009).

The mean elevation difference of active and inactive rock glaciers in the Poiqu River basin is rather minimal (~ 30m). In other regions like the Tyrolean Alps or in the Bolivian Andes, the difference is more pronounced (~100 m) (Krainer and Ribis 2012; Rangecroft *et al.* 2014). This can be attributed to several phenomena: the conservative classification approach to separate rock glaciers in active and inactive rock glaciers, the upward shift of the 0°C isotherm over time is less pronounced in the Poiqu region than in the other regions, or to the fact that topographic inactivity is more pronounced in our study region.

Active rock glaciers are commonly considered as indicators of the lower limit of discontinuous permafrost (Humlum 1998; Lilleøren and Etzelmüller 2011; Lilleøren *et al.* 2013; Scotti *et al.* 2013). From the lower limit of all active rock glaciers, we estimated the lower limit is at an elevation of approximately 4100 m asl. This is slightly less than the one found for the Himachal Himalaya (~4500 m) (Pandey 2019) but higher than in the Tien Shan where available data show the highest value in the Ak-Shirak range, Central Tien Shan (about 4020 m asl., (Bolch *et al.* 2019)) and clearly lower values in the outer ranges (northern Tien Shan in Kazakhstan: 3200 m, (Bolch and Gorbunov 2014); north-eastern Tien Shan in China ~2700 m (Wang *et al.* 2017)). On a global view, this is lower than the one found in the Bolivian Andes (4700 m asl.) and Chilean Andes (4400 m asl.) (Brenning 2005; Rangecroft *et al.* 2014), but higher than

parts of the Argentinean Andes at around 30° S (3600 m asl) (Esper Angillieri 2009) and the Tyrolean Alps (2500 m) (Krainer and Ribis 2012).

Most of the active rock glaciers can be found in the E and SW sectors. This pattern is thus different to the one found in the Nepalese Himalaya (Jones, Harrison, Anderson, Selley *et al.* 2018), north-eastern Tien Shan of China (Wang *et al.* 2017), the Himachal Himalaya (Pandey 2019), central Italy and southern Carpathians (Onaca *et al.* 2017; Scotti *et al.* 2013). The majority of the latter rock glacier inventories have a northerly aspect distribution signifying that slopes with lower potential incoming solar radiation are also the most suitable slopes for rock glacier development. In our case this is different and we believe that this pattern is mostly reducible to the topography and geometric factors in our study region (Aizen *et al.* 1995; Li and Li 2014). Looking at Fig. 1 it becomes obvious that the main mountain ridges have mostly a diagonal direction which forces the rock glaciers to develop either on the NE or SW part.(Jones, Harrison, Anderson, Selley *et al.* 2018), north-eastern Tien Shan of China (Wang *et al.* 2017), the inventory of rock glaciers in the Himachal Himalaya (Pandey 2019) central Italy and southern Carpathians (Onaca *et al.* 2017; Scotti *et al.* 2013). The majority of the latter rock glacier inventories have a northerly aspect distribution signifying that slopes with lower potential incoming solar radiation are also the most suitable slopes for rock glacier development. In our case this is different and we believe that this pattern is mostly reducible to the topography and geometric factors in our study region. Looking at Fig. 1 it becomes obvious that the main mountain ridges have mostly a diagonal direction which forces the rock glaciers to develop either on the NE or SW part.

We also found a strong correlation of the geographical locations on the altitude distribution for the whole sample. The mean elevations generally increase from south to north and decrease from the west until the main valley from where they start to increase

again. This correlation was also visible in the Tien Shan and Himachal Himalaya rock glacier inventory (Pandey 2019; Wang et al. 2017). In the latter one, the mean altitude per latitude decreased from south to north in contrast to our findings.

This dependence on the altitude should also be investigated together with the mean annual air temperature (MAAT). The facts that the MAAT also decreases with altitude and the precipitation regime gets drier towards the Tibetan Plateau, implies that booth climatic parameters may influence ground thermal conditions and thus the formation, evolution and survival of the rock glaciers similar as ground elsewhere (Barsch 1977; Haeberli 1983; Baroni *et al.* 2004). In response to the increasing continentality from south to north also the equilibrium line altitude (ELA) of the glaciers increases, expanding the niche for rock glacier development (Rangecroft *et al.* 2014). How much the characteristics of the contribution area (e.g., area, slope, headwall and elevation range, Bolch and Gorbunov 2014) plays a role in the distribution of the rock glaciers remains to be investigated.

For the first time, the frontal slopes of rock glaciers were mapped automatically for all identified rock glaciers. Our results indicated that slope angle of the front is lower for inactive rock glaciers as also shown elsewhere (Ikeda and Matsuoka 2002). The scatter, however, is considerable which indicates the heterogeneity of the rock glaciers but can in part also be attributed to the inaccuracies of the automated identification of the rock glacier fronts. Our investigation could not prove, that rock glaciers are classified in to active and inactive ones by the frontal slope only and the thresholds suggested in literature (Ikeda and Matsuoka 2002) are not ubiquitous. We also assume, that the thresholds are conditional to the lithology of a region (Krainer and Ribis 2012) and thus cannot be transferred directly to another region in the world.

The rock glacier inventory revealed also some potential hazards in combination with some lakes. We identified three sites which could potentially be hazardous due to a) future melt of the ice core of the rock glacier destabilising the "damming" landform or b) slope destabilisation due to seismic activities, avalanches or glacier break off in combination with a flood wave (Chen *et al.* 2019). Lake B, Cirenmaco lake, in the Zhangzangbo valley has already received negative public attention after its damaging 1981 outburst flood (Wang *et al.* 2015) and was also detected by an automated Tibet wide assessment as highly dangerous lake (Allen *et al.* 2019). However, a more detailed integrated hazard assessment is recommended to assess their hazard susceptibility and risk to the downstream areas.

Data and methodological constraints

The availability of very high optical resolution data in combination with a very high-resolution DEM (spatial resolution of 1m which is rarely available for a remote region like the Poiqu) was key for high accuracy. At the initial stage of our study the mapping was done using the best available free data sources: Sentinel 2 images with 10 m spatial resolution and a hillshade derived from the 8 m High Mountain Asia DEM (Shean 2017). Only on a later stage we could purchase tri-stereo Pléiades optical satellite imagery with a resolution of 0.5 m. After this re-assessment the numbers of rock glaciers reduced only slightly (by eight rock glaciers) but the area covered by the rock glaciers were reduced by about 50%. The main reason is that the higher resolution data enabled us to better identify the rock glacier boundaries especially in the upper areas of the rock glaciers and for rock glaciers without clearly identifiable distinct fronts and to better distinguish rock glaciers from similar looking landforms like rock fall deposits.

The availability of a very-high resolution DEM also enabled us to perform the automatic mapping of the frontal slopes of the rock glaciers. Only with such a DEM the slope break in the front of the rock glacier can, in combination with Object Based Image Analysis (OBIA), be mapped with the required precision.

Deriving uncertainties for rock glacier outlines is even more challenging as for glaciers with debris cover (Paul *et al.* 2013). This was confirmed by a multiple digitizing experiment performed by (Brardinoni *et al.* 2019) on rock glaciers in the Austrian Alps. This study shows a high inter-operator variability together with an increase in the number of mapped landforms when high resolution data are available.

In addition, Brardinoni *et al.* (2019) state that the variability of the mapped landforms is larger when mapping relict rock glaciers. This is because active and inactive rock glaciers still incorporate a high proportion of internal ice (may produce an arcuate ridge), whereas relict rock glaciers are ice-free, thus leading to a decrease in the frontal slope to the angle of repose.

In order to reduce the uncertainty and the subjectivity the mapping was performed at least three times and cross-checked with independent operators. In addition to that, we also converted the shape files to a kml file for further examination in Google Earth as successfully applied in other studies (Schmid *et al.* 2015).

Nevertheless, the mapping of the rooting zone and their separation to the headwall remained most challenging. In order to be consistent, we removed areas in the rooting zone if they were larger than 35°.

The number of active rock glaciers (ARGs) we compiled is a conservative estimate due to the following reasons: First, we may have missed some ARGs due to the geometric distortions such as shadows and layovers in the SAR signal. Second ARGs facing nearly north or south might have been also missed, as InSAR is not sensitive to

ground motions along these directions. Finally, some small ARGs could not be identified as the interferogram maps have a moderate resolution of about 15 m (cf. Wang *et al.* 2017). Nevertheless, the InSAR approach has been proven useful and was also applied elsewhere to assess rock glacier activity (e.g., Barboux *et al.* 2014).

In many cases field knowledge helps to aid rock glacier delineation and to assess their kinematic status, but this is time consuming, costly and often also dangerous. As such, an automated methodology is needed that the mapping is more objective and traceable. In the recent years new methods have been developed, to better discriminate between active and inactive rock glaciers by backscatter and coherence rasters (Bertone *et al.* 2019) or by logistic regression, support vector machine and random forest classifier (Kofler *et al.* 2020). Robson *et al.* (2020) used deep learning with object-based image analysis to map rock glaciers over regional scales with promising results as the amount of manual work was significantly reduced.

7. Conclusion

The results of our inventory for the Poiqu River basin reveal in total 370 rock glaciers (148 active and 222 inactive) covering an area of about 20.9 km2 for the year 2018. The rock glaciers are located between ~4000 m and ~6000 m with a mean altitude of ~5100 m a.s.l. and face mostly towards the East (17%) and Southwest (16%). The mean overall slope of all rock glaciers is close 19.3° (active: 19.7°, inactive: 19.0°). We also found nine rock glaciers damming lakes, of which three of them could potentially be dangerous.

However, accurate mapping rock glaciers and identification of their activity is challenging and high-resolution data is key in this regard. The acquisition of very high resolution optical stereo satellite data and the derived DEM allowed us to identify map

even small rock glaciers in the study region. The use of InSAR supported the distinguishing between active and inactive rock glaciers.

The available high resolution data sets enabled us to develop of a method to automatically map the front slopes of the rock glaciers based on an object-based approach and subsequently derive their mean slopes in order to get an indication of their activity. We could confirm that active rock glaciers have overall steeper slopes than inactive ones when considering all rock glaciers with a mean frontal slope of greater than 30°.

The generated rock glacier inventory is of high accuracy and an important baseline data set can for modelling purposes or estimations of the hydrological importance.

Conflict of interest

Philipp Rastner was partly employed by the company GeoVille Information Systems and Data Processing GmbH. The remaining authors declare that the research was conducted in the absence of any commercial or financial relationships that could be construed as a potential conflict of interest.

Author contribution statement

PR and TB designed the study. PR mapped the rock glaciers, analysed data, developed the algorithm to map the frontal slopes and wrote the manuscript. TB contributed to the mapping and analysis. AB processed the Pléiades data, YH and LL processed the InSAR data. PR, TB, YH/LL and AB wrote the draft of the manuscript. All authors contributed to the final version of the manuscript.

Funding

This study was conducted within the framework of the Dragon 4 program funded by ESA (4000121469/17/I-NB) and further supported by the Strategic Priority Research Program of Chinese Academy of Sciences (XDA20100300), Swiss National Science Foundation (Grant No. IZLCZ2_169979/1) and the Hong Kong Research Grants Council (CUHK14303417 and HKPFS PF16-03859).

Acknowledgements

The Pléiades data used in this study was purchased within the ISIS programm © CNES 2018 and Airbus D&S 2018, all rights reserved. The ALOS-1 PALSAR data are copyrighted and provided by the Japan Aerospace Exploration Agency through the EO-RA2 project ER2A2N081. We acknowledge Dr. Simon Allen from the Geography Department at the University of Zurich for his constructive comments on the data.

Data availability:

The rock glacier inventory will be available from PANGAEA and www.mountcryo.org

References

Aizen, V.B., Aizen, E.M. and Melack, J.M., 1995. Climate, snow cover and runoff in the Tien Shan. *Water Resources Bulletin*, 31 (6), 1113–1129. [In English]

Allen, S.K., Zhang, G., Wang, W., Yao, T. and Bolch, T., 2019. Potentially dangerous glacial lakes across the Tibetan Plateau revealed using a large-scale automated assessment approach. *Science Bulletin*, 64, 435–445. doi: 10.1016/j.scib.2019.03.011

Barboux, C., Delaloye, R. and Lambiel, C., 2014. Inventorying slope movements in an Alpine environment using DInSAR. *Earth Surface Processes and Landforms*, 39, 2087–2099. doi: 10.1002/esp.3603

Baroni, C., Carton, A. and Seppi, R., 2004. Distribution and behaviour of rock glaciers in the Adamello–Presanella Massif (Italian Alps). *Permafrost and Periglacial Processes*, 15 (3), 243–259. doi: 10.1002/ppp.497

Barsch, D., 1977. Alpiner Permafrost: ein Beitrag zur Verbreitung, zum Charakter und zur Ökologie am Beispiel der Schweizer Alpen. In: Poser, H. (ed.), *Formen, Formengesellschaften und Untergrenzen in den heutigen periglazialen Höhenstufe der Hochgebirge Europas und Afrikas zwischen Arktis und Äquator*, 31. Abh. der Akademie der Wissenschaften in Göttingen. 118–141.

Barsch, D., 1996. *Rockglaciers: Indicators for the present and former geoecology in high mountain environments*. Physical Environment. Springer, Berlin. 331 p.

Berger, J., Krainer, K. and Mostler, W., 2004. Dynamics of an active rock glacier (Ötztal Alps, Austria). *Quaternary Research*, 62 (3), 233–242. doi: 10.1016/j.yqres.2004.07.002

Berthling, I., 2011. Beyond confusion: Rock glaciers as cryo-conditioned landforms. *Geomorphology*, 131 (3-4), 98–106. doi: 10.1016/j.geomorph.2011.05.002

Bertone, A., Zucca, F., Marin, C., Notarnicola, C., Cuozzo, G., Krainer, K., Mair, V., Riccardi, P., Callegari, M. and Seppi, R., 2019. An unsupervised method to detect rock glacier activity by using Sentinel-1 SAR interferometric coherence: a regional-scale study in the eastern European Alps. *Remote Sensing*, 11 (14), 1711.

Bishop, M.P., Barry, R.G., Bush, A.B.G., Copeland, L., Dwyer, J.L., Fountain, A.G., Haeberli, W., Hall, D.K., Kääb, A., Kargel, J.S., Molnia, B.F., Olsenholler, J.A., Paul, F., Raup, B.H., Shroder, J.F., Trabant, D.C. and Wessels, R., 2004. Global

Land Ice Measurements from Space (GLIMS): Remote sensing and GIS investigations of the Earth's cryosphere. *Geocarto International*, 19 (2), 57–85.

Blagbrough, J.W. and Farkas, S.E., 1968. Rock glaciers in the San Mateo. Mountains, south-central New Mexico. *American Journal of Science*, 266 (9), 812–823. doi: 10.2475/ajs.266.9.812

Blöthe, J.H., Rosenwinkel, S., Höser, T. and Korup, O., 2019. Rock-glacier dams in High Asia. *Earth Surface Processes and Landforms*, 44 (3), 808–824. doi: 10.1002/esp.4532

Bolch, T. and Gorbunov, A.P., 2014. Characteristics and origin of rock glaciers in Northern Tien Shan (Kazakhstan/Kyrgyzstan). *Permafrost and Periglacial Processes*, 25 (4), 320–332. doi: 10.1002/ppp.1825

Bolch, T. and Marchenko, S.S., 2009. Significance of glaciers, rockglaciers and ice-rich permafrost in the Northern Tien Shan as water towers under climate change conditions. In: Braun, L., Hagg, W., Severskiy, I.V. and Young, G.J. (eds), *Selected papers from the Workshop "Assessment of Snow, Glacier and Water Resources in Asia" held in Almaty, Kazakhstan, 28-30 Nov. 2006. IHP/HWRP-Berichte 8*. 132–144.

Bolch, T., Rohrbach, N., Kutuzov, S., Robson, B.A. and Osmonov, A., 2019. Occurrence, evolution and ice content of ice-debris complexes in the Ak-Shiirak, Central Tien Shan revealed by geophysical and remotely-sensed investigations. *Earth Surface Processes and Landforms*, 44 (1), 129–143. doi: 10.1002/esp.4487

Bollmann, E., Girstmair, A., Mitterer, S., Krainer, K., Sailer, R. and Stötter, J., 2015. A rock glacier activity index based on rock glacier thickness changes and displacement rates derived from airborne laser scanning. *Permafrost and Periglacial Processes*, 26 (4), 347–359. doi: 10.1002/ppp.1852

Brardinoni, F., Scotti, R., Sailer, R. and Mair, V., 2019. Evaluating sources of uncertainty and variability in rock glacier inventories. *Earth Surface Processes and Landforms*, 44 (12), 2450–2466. doi: 10.1002/esp.4674

Brenning, A., 2005. Geomorphological, hydrological and climatic significance of rock glaciers in the Andes of Central Chile (33-35°S). *Permafrost and Periglacial Processes*, 16 (3), 231–240.

Brighenti, S., Tolotti, M., Bruno, M.C., Engel, M., Wharton, G., Cerasino, L., Mair, V. and Bertoldi, W., 2019. After the peak water: the increasing influence of rock glaciers on alpine river systems. *Hydrological Processes*, 33 (21), 2804–2823.

Burger, K.C., DegenhardtJr, J.J. and Giardino, J.R., 1999. Engineering geomorphology of rock glaciers. *Geomorphology*, 31 (1-4), 93.

Chen, N., Liu, M., Deng, M., Iqbal, J., Hu, G., Wahid, S., Liu, W. and Han, D., 2019. The incision variations of Poiqu documented by the Zhangmu landslide in the Upper Himalaya of Tibet. *Advancing Pleistocene and Holocene climate change research in the Carpathian-Balkan region*, 532, 66–74. doi: 10.1016/j.quaint.2019.09.040

Cremonese, E., Gruber, S., Phillips, M., Pogliotti, P., Boeckli, L., Noetzli, J., Suter, C., Bodin, X., Crepaz, A., Kellerer-Pirklbauer, A., Lang, K., Letey, S., Mair, V., Di Morra Cella, U., Ravanel, L., Scapozza, C., Seppi, R. and Zischg, A., 2011. Brief Communication: "An inventory of permafrost evidence for the European Alps". *The Cryosphere*, 5 (3), 651–657. doi: 10.5194/tc-5-651-2011

Durand, A., Michel, J., Franchis, C. de, Allenbach, B. and Giros, A., 2013. Qualitative assessment of four DSM generation approaches using Pleiades-HR data. In: Lasaponara, R., Masini, N. and Biscione, M. (eds), *33rd EARSeL Symposium Towards Horizon 2020*, 3-6 June 2013, Matera, Italy. 4999-510.

Esper Angillieri, M.Y., 2009. A preliminary inventory of rock glaciers at 30°S latitude, Cordillera Frontal of San Juan, Argentina. *Hurricanes and Typhoons: From the Field Records to the Forecast*, 195 (1), 151–157. doi: 10.1016/j.quaint.2008.06.001

Falaschi, D., Castro, M., Masiokas, M., Tadono, T. and Ahumada, A.L., 2014. Short communication: Rock glacier inventory of the Valles Calchaquíes Region (~ 25°S), Salta, Argentina, derived from ALOS data. *Permafrost and Periglacial Processes*, 25, 69–75.

Falaschi, D., Tadono, T. and Masiokas, M., 2015. Rock glaciers in the Patagonian Andes: an inventory for the Monte San Lorenzo (Cerro Cochrane) Massif, 47° S. *Geografiska Annaler A*. doi: 10.1111/geoa.12113

Farr, T.G., Rosen, P.A., Caro, E., Crippen, R., Duren, R., Hensley, S., Kobrick, M., Paller, M., Rodriguez, E., Roth, L., Seal, D., Shaffer, S., Shimada, J., Umland, J., Werner, M., Oskin, M., Burbank, D. and Alsdorf, D., 2007. The Shuttle Radar Topography Mission. *Review of Geophysics*, 45 (2), RG2004.

Gleyzes, M.A., Perret, L. and Kubik, P., 2012. Pleiades system architecture and main performances. *International Archives of the Photogrammetry, Remote Sensing and Spatial Information Sciences*, 39 (1), 537–542.

Gorbunov, A.P., Seversky, E.V., Titkov, S.N., Marchenko, S.S. and Popov, M., 1998. Rock glaciers, Zailiysiky Range, Kungei Ranges, Tienshan, Kazakhstan, Version 1. [Indicate subset used]. Boulder, Colorado USA. NSIDC: National Snow and Ice Data Center. [Date Accessed].

Gorbunov, A.P. and Titkov, S.N., 1989. *Kamennye Gletchery Gor Srednej Azii: (=Rock glaciers of the Central Asian mountains)*. Akademia Nauk SSSR, Irkutsk.

Gorbunov, A.P., Titkov, S.N. and Polyakov, V.G., 1992. Dynamics of the rock glaciers of the Northern Tien Shan and the Djungar Alatau, Kazakhstan. *Permafrost and Periglacial Processes*, 3, 29–39.

Haeberli, W., 1983. Permafrost-glacier relationships in the Swiss Alps-today and in the past. In: *4th International Conference on Permafrost*. *4th International Conference of Permafrost*. National Academy Press, Washington, DC. 415–420.

Haeberli, W., Hallet, B., Arenson, L.U., Elconin, R., Humlum, O., Kääb, A., Kaufmann, V., Ladanyi, B., Matsuoka, N., Springman, S. and Vonder Mühll, D., 2006. Permafrost creep and rock glacier dynamics. *Permafrost and Periglacial Processes*, 17 (3), 189–214. doi: 10.1002/ppp.561

Humlum, O., 1998. The climatic significance of rock glaciers. *Permafrost and Periglacial Processes*, 9 (4), 375–395. doi: 10.1002/(SICI)1099-1530(199810/12)9:4<375::AID-PPP301>3.0.CO;2-0

Humlum, O., 2000. The geomorphic significance of rock glaciers: estimates of rock glacier debris volumes and headwall recession rates in West Greenland. *Geomorphology*, 35, 41–67.

Ikeda, A. and Matsuoka, N., 2002. Degradation of talus-derived rock glaciers in the Upper Engadin, Swiss Alps. *Permafrost and Periglacial Processes*, 13 (2), 145–161.

Imhof, M., 1996. Modelling and verification of the permafrost distribution in the Bernese Alps (Western Switzerland). *Permafrost and Periglacial Processes*, 7 (3), 267–280. doi: 10.1002/(SICI)1099-1530(199609)7:3<267::AID-PPP221>3.0.CO;2-L

IPA Action Group, 2020. *IPA Action Group Rock glacier inventories and kinematics: Towards standard guidelines for inventorying rock glaciers: Baseline concepts (Version 4.1)*.

Jones, D.B., Harrison, S., Anderson, K. and Betts, R.A., 2018. Mountain rock glaciers contain globally significant water stores. *Scientific Reports*, 8, 2834. doi: 10.1038/s41598-018-21244-w

Jones, D.B., Harrison, S., Anderson, K., Selley, H.L., Wood, J.L. and Betts, R.A., 2018. The distribution and hydrological significance of rock glaciers in the Nepalese Himalaya. *Global and Planetary Change*, 160 (Supplement C), 123–142. doi: 10.1016/j.gloplacha.2017.11.005

Kääb, A., Haeberli, W. and Gudmundsson, G.H., 1997. Analysing the creep of mountain permafrost using high precision aerial photogrammetry: 25 years of monitoring Gruben rock glacier, Swiss Alps. *Permafrost and Periglacial Processes*, 8 (4), 409–426. doi: 10.1002/(SICI)1099-1530(199710/12)8:4<409::AID-PPP267>3.0.CO;2-C

Kääb, A., Huggel, C., Fischer, L., Guex, S., Paul, F., Roer, I., Salzmann, N., Schlaefli, S., Schmutz, K., Schneider, D., Strozzi, T. and Weidmann, Y., 2005. Remote sensing of glacier- and permafrost-related hazards in high mountains: an overview. *Natural Hazards and Earth System Science*, 5, 527–554. [In Englisch]

Kääb, A., Strozzi, T., Bolch, T., Caduff, R., Trefall, H., Stoffel, M. and Kokarev, A., 2021. Inventory and changes of rock glacier creep speeds in Ile Alatau and Kungöy Ala-Too, northern Tien Shan, since the 1950s. *The Cryosphere*, 15 (2), 927–949. doi: 10.5194/tc-15-927-2021

Kellerer-Pirklbauer, A., Lieb, G.K. and Kleinferchner, H., 2012. A new rock glacier inventory of the eastern European Alps. *Austrian Journal of Earth Sciences*, 105, 78–93.

Khanal, N.R., Hu, J.-M. and Mool, P., 2015. Glacial lake outburst flood risk in the Poiqu/Bhote Koshi/Sun Koshi River Basin in the Central Himalayas. *Mountain*

Research and Development, 35 (4), 351–364. doi: 10.1659/MRD-JOURNAL-D-15-00009

Kofler, C., Steger, S., Mair, V., Zebisch, M., Comiti, F. and Schneiderbauer, S., 2020. An inventory-driven rock glacier status model (intact vs. relict) for South Tyrol, Eastern Italian Alps. *Geomorphology*, 350, 106887. doi: 10.1016/j.geomorph.2019.106887

Krainer, K. and Ribis, M., 2012. A rock glacier inventory of the Tyrolean Alps (Austria). *Austrian Journal of Earth Sciences*, 105, 32–47.

Li, J., Pan, Z. and Feng, X.e.a., 2006. Magnetic fabrics and tectonic implications of the Higher Himalayan rocks in Nyalam, southern Tibet. *Chinese Journal of Geophysics*, 49 (2), 496–503.

Li, Y. and Li, Y., 2014. Topographic and geometric controls on glacier changes in the central Tien Shan, China, since the Little Ice Age. *Annals of Glaciology*, 55 (66), 177–186. doi: 10.3189/2014AoG66A031

Lilleøren, K.S. and Etzelmüller, B., 2011. A regional inventory of rock glaciers and ice-cored moraines in norway. *Geografiska Annaler A*, 93 (3), 175–191. doi: 10.1111/j.1468-0459.2011.00430.x

Lilleøren, K.S., Etzelmüller, B., Gärtner-Roer, I., Kääb, A. and Westermann, S., 2013. The distribution, thermal characteristics and dynamics of permafrost in Tröllaskagi, Northern Iceland, as Inferred from the distribution of rock glaciers and ice-cored moraines. *Permafrost and Periglacial Processes*, 24, 322–335. doi: 10.1002/ppp.1792

Necsoiu, M., Onaca, A., Wigginton, S. and Urdea, P., 2016. Rock glacier dynamics in Southern Carpathian Mountains from high-resolution optical and multi-temporal SAR satellite imagery. *Remote Sensing of Environment*, 177, 21–36.

Onaca, A., Ardelean, F., Urdea, P. and Magori, B., 2017. Southern Carpathian rock glaciers: Inventory, distribution and environmental controlling factors. *Geomorphology*, 293, 391–404. doi: 10.1016/j.geomorph.2016.03.032

Pandey, P., 2019. Inventory of rock glaciers in Himachal Himalaya, India using high-resolution Google Earth imagery. *Glacial Landscape Evolution - Implications for Glacial Processes, Patterns and Reconstructions*, 340, 103–115. doi: 10.1016/j.geomorph.2019.05.001

Paul, F., Barrand, N.E., Baumann, S., Berthier, E., Bolch, T., Casey, K.A., Frey, H., Joshi, S.P., Konovalov, V., LeBris, R., Mölg, N., Nosenko, G., Nuth, C., Pope, A., Racoviteanu, A., Rastner, P., Raup, B., Scharrer, K., Steffen, S. and Winsvold, S., 2013. On the accuracy of glacier outlines derived from remote sensing data. *Annals of Glaciology*, 54 (63), 171–182.

Rangecroft, S., Harrison, S., Anderson, K., Magrath, J., Castel, A.P. and Pacheco, P., 2014. A first rock glacier inventory for the Bolivian Andes. *Permafrost and Periglacial Processes*, 25 (4), 333–343. doi: 10.1002/ppp.1816

Reinosch, E., Gerke, M., Riedel, B., Schwalb, A., Ye, Q. and Buckel, J., 2021. Rock glacier inventory of the western Nyainqêntanglha Range, Tibetan Plateau, supported by InSAR time series and automated classification. *Permafrost and Periglacial Processes*, n/a (n/a). doi: 10.1002/ppp.2117

Robson, B.A., Bolch, T., MacDonell, S., Hölbling, D., Rastner, P. and Schaffer, N., 2020. Automated detection of rock glaciers using deep learning and object-based image analysis. *Remote Sensing of Environment*, 250, 112033. doi: 10.1016/j.rse.2020.112033

Rosen, P.A., Gurrola, E., Sacco, G.F. and Zebker, H.A., 2012. The InSAR scientific computing environment. In: *EURSAR 2012*. *9th European Conference on Synthetic Aperture Radar*, Nuremberg, Germany. VDE. 730–733.

Sattler, K., Anderson, B., Mackintosh, A., Norton, K. and Róiste, M. de, 2016. Estimating permafrost distribution in the maritime Southern Alps, New Zealand, based on climatic conditions at rock glacier sites. *Frontiers in Earth Science*, 4, 4. doi: 10.3389/feart.2016.00004

Schmid, M.-O., Baral, P., Gruber, S., Shahi, S., Shrestha, T., Stumm, D. and Wester, P., 2015. Assessment of permafrost distribution maps in the Hindu Kush Himalayan region using rock glaciers mapped in Google Earth. *The Cryosphere*, 9 (6), 2089–2099. doi: 10.5194/tc-9-2089-2015

Schoeneich, P., Bodin, X., Echelard, T., Kaufmann, V., Kellerer-Pirklbauer, A., Krysiecki, J.-M. and Lieb, G.K., 2015. Velocity changes of rock glaciers and induced hazards. In: Lollino, G., Manconi, A., Clague, J.J., Shan, W. and Chiarle, M. (eds), *Engineering Geology for Society and Territory: - Volume 1*, 1. Springer, Cham.

Scotti, R., Brardinoni, F., Alberti, S., Frattini, P. and Crosta, G.B., 2013. A regional inventory of rock glaciers and protalus ramparts in the central Italian Alps. *Geomorphology*, 186 (0), 136–149. doi: 10.1016/j.geomorph.2012.12.028

Shean, D.E., 2017. High Mountain Asia 8-meter DEM mosaics derived from optical imagery, version 1. doi: 10.5067/KXOVQ9L172S2.

Strozzi, T., Caduff, R., Jones, N., Barboux, C., Delaloye, R., Bodin, X., Kääb, A., Mätzler, E. and Schrott, L., 2020. Monitoring rock glacier kinematics with satellite Synthetic Aperture Radar. *Remote Sensing*, 12 (3). doi: 10.3390/rs12030559

Titkov, S.N., 1988. Rock Glaciers and glaciation of the Central Asian Mountains. In: *Proceedings of the 5th International Permafrost Conference, Vol. 1*, Trondheim, 1. Tapir Publishers. 259-262. 259–262.

Wahrhaftig, C. and Cox, A., 1959. Rock Glaciers in the Alaska Range. *Bull.Geol.Soc. of America*, 70 (4), 383–436.

Wang, W., Gao, Y., Anacona, P.I., Lei, Y., Xiang, Y., Zhang, G., Li, S. and Lu, A., 2015. Integrated hazard assessment of Cirenmaco glacial lake in Zhangzangbo valley, Central Himalayas. *Geomorphology*. doi: 10.1016/j.geomorph.2015.08.013

Wang, X., Liu, L., Zhao, L., Wu, T., Li, Z. and Liu, G., 2017. Mapping and inventorying active rock glaciers in the northern Tien Shan of China using satellite SAR interferometry. *The Cryosphere*, 11 (2), 997–1014. doi: 10.5194/tc-11-997-2017

Zhang, G., Bolch, T., Allen, S., Linsbauer, A., Chen, W. and Wang, W., 2019. Glacial lake evolution and glacier–lake interactions in the Poiqu River basin, central Himalaya, 1964–2017. *Journal of Glaciology*, 65 (251), 347–365. doi: 10.1017/jog.2019.13